Journal of Materials Chemistry

Cite this: J. Mater. Chem., 2011, 21, 17098

www.rsc.org/materials

PAPER

Evidence of a polar cybotactic smectic A phase in a new fluorine substituted bent-core compound†

Mamatha Nagaraj,[a] Anne Lehmann,[b] Marko Prehm,[b] Carsten Tschierske[b] and Jagdish K. Vij*[a]

Received 6th July 2011, Accepted 24th August 2011
DOI: 10.1039/c1jm13140k

The mesomorphic properties of an achiral, fluorine substituted bent-core liquid crystal have been investigated using polarising optical microscopy, electro-optics, X-ray diffraction and dielectric spectroscopy. A new phase, designated as CybAP$_A$, has been found. This phase is a cluster phase consisting of microscopic enlarged antiferroelectric smectic A type clusters. The CybAP$_A$ phase is observed below a SmA phase and exists irrespective of the alignment layer and the cell thickness. The CybAP$_A$ phase behaves like a nematic phase with low viscosity and exhibits thermal fluctuations. But on applying an electric field, it shows smectic-like textures and exhibits tristable antiferroelectric switching. X-Ray diffraction of aligned samples of this phase confirms the non-tilted orientation of the major director and long range 1D positional order of the molecules. The dielectric spectroscopic studies show the appearance of strong dipolar correlations on approaching the CybAP$_A$ phase from the higher temperature SmA phase, confirming the formation of SmAP$_A$ clusters, which is associated with the onset of phase biaxiality. This provides a significant step forward to achieve the illusive orthorhombic biaxial cybotactic nematic phase from bent-core molecules.

1. Introduction

Bent-core mesogens are generally made up of a bent aromatic core and two flexible side chains. Research in bent-core liquid crystalline systems has emerged as one of the major areas of investigations in liquid crystals. This is due to a wide range of unique phase structures that have been found for bent-core materials. Bent-core liquid crystals show a range of interesting properties, for example they exhibit chiral superstructures even though the molecules are achiral, spontaneous polar ordering, unusual rheological properties and giant flexoelectricity.[1–3]

In 1992 Brand *et al.*[4] suggested a model of ferroelectricity in non-tilted smectic phases formed by achiral bent-core molecules. In bent-core mesogens, the steric moment caused by the molecular geometry (or the breaking of rotational symmetry about the molecular principal axis) induces polar packing within the smectic layer, which gives rise to the polarisation in the bow-axis direction and this creates local C_{2v} symmetry. These types of phases are called orthogonal polar smectic phases. They mainly include SmAP$_R$,[5] SmAP$_A$,[6–9] SmAP$_{AR}$[10] and SmAP$_F$[11] phases (where R stands for random, A for antiferroelectric and F for ferroelectric). Also, non-polar biaxial orthogonal smectic phases with interdigitated layers are found to exist in bent-core and in dimer systems.[12–14]

Freiser in 1970[15] predicted that a reduction in the molecular symmetry, in liquid crystals, could lead to the formation of a biaxial nematic (N$_b$) phase in addition to the uniaxial nematic (N$_u$) phase. Bent-core molecules are considered to be one of the potential candidates to achieving the thermotropic N$_b$ phase, even though there is an on-going debate on the existence of the spontaneous biaxial nematic phase in the bent-core liquid crystals. Many results suggest the existence of microscopic aggregation of smectics such as SmA, SmC, *etc.* in the nematic phase. Such a nematic phase is called cybotactic nematic and is represented as N$_{cyb}$.[16–18] In some materials, when we go down in temperature from the N$_{cyb}$ phase, clusters of smectic types grow in size and before reaching the smectic phases themselves these clusters get elongated with relatively long correlation lengths. These intermediate phases, unknown in liquid crystal phases of rod-like molecules, are tentatively designated as cybotactic phases (and are labelled as CybA, CybC, *etc.*), which under electric/magnetic field or surface treatment align to give rise to the various smectic phases.[18,19] Previously reported cybotactic phases and most of the N$_{cyb}$ phases are formed by SmC-type clusters. From the point of view of applications in displays, cybotactic nematic phases composed of smectic cybotactic clusters with non-tilted and polar organisation of the molecules would be of significant interest as these phases can be considered as biaxial nematics of the orthorhombic type.[17]

[a]*Department of Electronic and Electrical Engineering, Trinity College, University of Dublin, Dublin 2, Ireland. E-mail: jvij@tcd.ie*
[b]*Organic Chemistry, Institute of Chemistry, Martin-Luther-University Halle-Wittenberg, D-06120 Halle, Germany*
† Electronic supplementary information (ESI) available. See DOI: 10.1039/c1jm13140k

In the literature, there are some reports about unusual phase transitions between distinct nematic phases. In some bent-core compounds, a second nematic phase, below the uniaxial nematic phase, has been reported. Schröder *et al.*[20] showed a phase sequence on cooling of N_u to N_X to Col_r (rectangular columnar phase). The textural features of the N_X phase were indicative of a smectic phase, but in contrast, a diffuse scattering in the small angle X-ray diffraction suggested a structure without any long-range positional order. Based on these observations, they had proposed a molecular model for the N_X phase in which the molecules are stacked along the bow-axis direction in bundles of non-defined dimensions. In between the bundles only a short range positional order exists and the neighbouring bundles are antiparallel to each other to prevent the macroscopic polarisation from being finite.

Keith *et al.* reported a tilted cluster phase assigned as CybC which occurs at the transition from the N_{cybC} phase to a SmC phase of compounds related to the compound studied in this paper, but without the fluorine substituents.[19] Based on results of X-ray diffraction (XRD) and textures, it was concluded that at the transition from N_{cybC} to CybC, the cybotactic clusters fuse to form elongated ribbon-like aggregates. The latter phase is distinct from N_{cybC} as a result of long range orientation correlation between the clusters, leading to phase biaxiality. CybC is distinct from proper SmC phases as the clusters are not yet fused to form quasi-infinite layers.

In this paper, a novel orthogonal polar cluster phase is reported and its mesomorphic properties are studied by polarising optical microscopy, electro-optics, X-ray diffraction and dielectric spectroscopy. This phase, designated as $CybAP_A$, is observed in a fluorine substituted achiral bent-core compound. The high temperature phase is a N_{cybA} phase, which on cooling forms a SmA phase first and then changes to the $CybAP_A$ phase. This phase possesses very low viscosity, and exhibits thermal fluctuations and, on applying the electric field, it shows smectic-like textures and exhibits tristable antiferroelectric switching.

2. Results and discussion

2.1 Synthesis

The synthetic approach to prepare the studied bent-core compound, PAL21, is shown in Scheme 1. For the synthesis of the target compound, 4-cyanoresorcinol (**1**)[21] was acylated with 4-(3-fluoro-4-octyloxybenzoyloxy)benzoic acid (**2**), which was obtained according to the methods described in the literature.[22] For details and analytical data see ESI†.

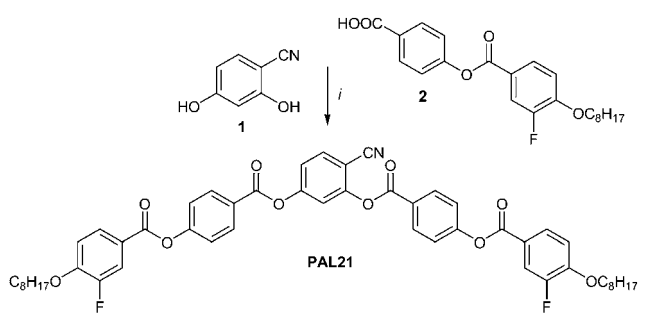

Scheme 1 Synthesis of PAL21: *reagents i*; (1) $SOCl_2$; (2) **1**, Et_3N, CH_2Cl_2, and pyridine.

2.2 Mesomorphic properties

The studied mesogen, PAL21, is a 4-cyanoresorcinol derivative containing fluorine atoms on the outer phenyl rings *ortho* to the *n*-alkoxy chain. It is an achiral bent-core molecule and shows negative dielectric anisotropy throughout the liquid crystal phase temperature range. PAL21 exhibits four mesophases on cooling: I → *phase-1* → *phase-2* → *phase-3* → *phase-4*. Based on the mesomorphic properties, we characterise these phases one by one. In this phase sequence, *phase-3* is the new phase of special interest and this phase will be discussed in more detail. Finally we characterise the phase sequence of PAL21 as: Cr *108 °C [33]* (M *97 °C [5.4]* $CybAP_A$ *100 °C [<0.02]*) SmA *112 °C [<0.02]* N_{cybA} *118 °C [1.0]* I (Cr = crystalline solid, I = isotropic liquid, M = crystalline mesophase; the abbreviations of the LC phases are explained in the text), where the values within the square brackets give the enthalpy of phase transition in kJ mol^{-1}, determined using differential scanning calorimetry (DSC) measurements (Fig. S2 in the ESI†).

The physical properties of bent-core mesogens with a resorcinol central unit and a fluorine substituted outer phenyl ring, but without the –CN group at the resorcinol core, have already been investigated[23,24] and also the mesomorphic properties as a function of the position of the fluorine atom in the molecule had also been studied in detail.[25] These studies showed the importance of dipolar interactions in influencing the occurrence of a particular columnar and ferroelectric or antiferroelectric switching smectic mesophase in five-ring esters. 4-Cyanoresorcinol bisbenzoates have also been investigated and they were found to produce cybotactic nematic phases with SmC clusters, CybC and $SmC/SmCP_A$ phases.[19,26] SmA and $SmAP_A$ phases were observed for 4-cyanoresorcinol benzoates with two reversed ester groups.[27] Herein fluoro substitution at the periphery is combined with –CN substitution at the apex to modify the mesophase structure.

Fig. 1 shows the polarising optical micrographs and Fig. 2 shows the 2D XRD patterns, χ-scans, and 2θ-scans of PAL21 of a magnetically aligned sample for different temperatures.

On cooling the sample in a planar cell, from the isotropic phase below $T = 118$ °C, we see *phase-1* (Fig. 1a), which shows schlieren textures of 2- and 4-brush declinations between untreated glass plates and possesses thermal fluctuations, characteristic of a uniaxial nematic phase. In a homeotropic alignment of the sample, this phase appears completely dark under crossed polarisers. In the XRD pattern a diffuse wide angle scattering with a maximum at $d = 0.46$ nm is centred on the equator (Fig. 2a and b). This indicates a liquid crystalline phase and that the alignment of the aromatic cores is parallel to the meridian (parallel to the magnetic field direction). In addition, there is a diffuse small angle scattering with a maximum at $d = 4.26$ nm which is centred on the meridian (Fig. 2c). The intensity of the small angle scattering is significantly higher than that of the diffuse wide angle scattering (see the inset in Fig. 2d). This confirms this phase to be a cybotactic nematic phase with SmA type clusters. Hence, *phase-1* is ascertained to be N_{cybA}.

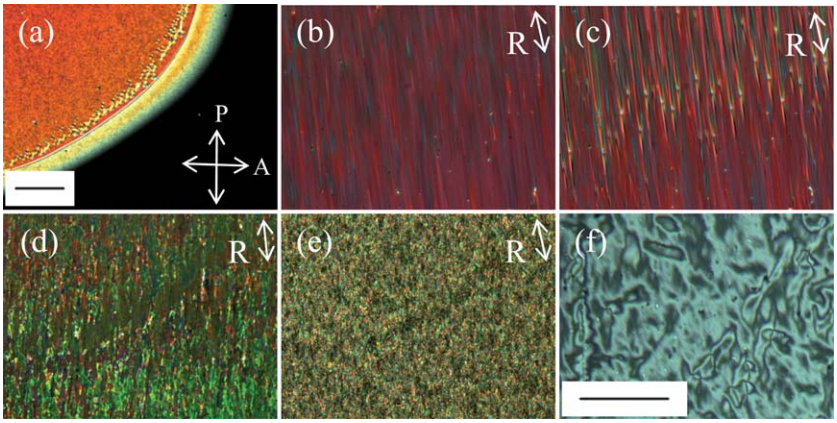

Fig. 1 POM textures of a planar cell of thickness 11 μm under crossed polarisers (a) isotropic to nematic phase transition at 118 °C (b) *phase-2* (SmA) at 110 °C (c) *phase-2* (SmA) at 102 °C, (d) *phase-3* ($CybAP_A$) at 98.5 °C, (e) *phase-4* (M) at 96 °C and (f) *phase-3* ($CybAP_A$) at 98.5 °C in a homeotropic cell. The length of the black line is 300 μm. P, A and R are the directions of polariser, analyser and rubbing.

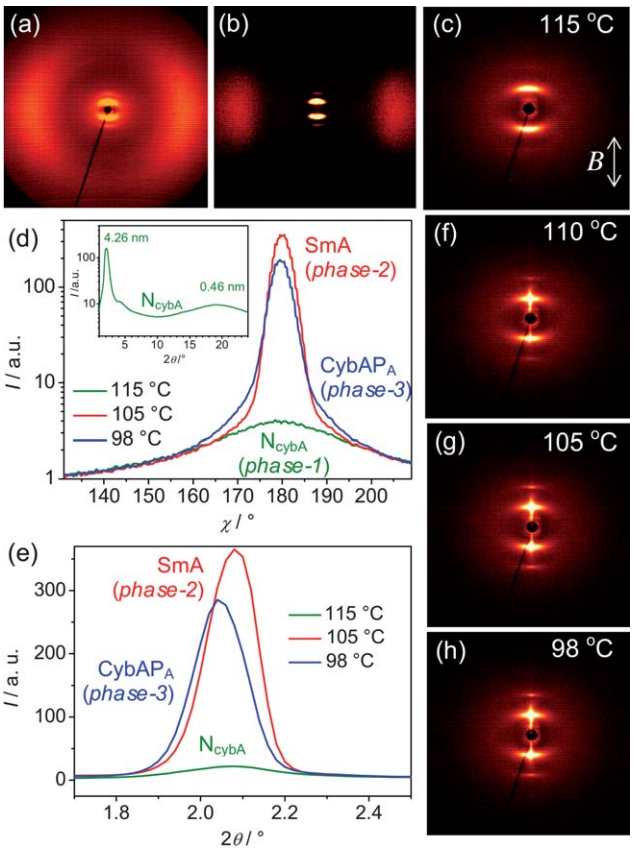

Fig. 2 (a) 2D diffraction pattern of PAL21 in the N_{cybA} phase at 105 °C, (b) same pattern after subtraction of the scattering from the isotropic ($T = 125$ °C); (c) small angle diffraction pattern; (d) comparison of χ-scan and (e) 2θ-scans over the small angle scattering of the three distinct LC phases; (f)–(h) show small angle diffraction patterns at the indicated temperatures; (f) and (g) the SmA phase and (h) the $CybAP_A$ phase. ***B*** is the direction of the magnetic field.

On further cooling the sample down to 112 °C, we reach *phase-2*, which is more viscous than the N_{cybA} phase (Fig. 1b). The sample appears dark in a homeotropic cell under crossed polarisers in *phase-2*. There is no transition enthalpy found for this phase transition in DSC (Fig. S2†). For a slightly higher temperature above this phase transition (say at 113 °C) one could induce *phase-2* from the N_{cybA} phase by applying a small electric field perpendicular to the major director. In the XRD pattern of this phase the position and shape of the diffuse wide angle scattering do not change and also the small angle scattering retains its position on the meridian with a *d*-value very similar to that in the N_{cybA} phase, indicating a non-tilted molecular director (Fig. 2f and g). The dependence of the layer reflection on temperature for PAL21 is shown in Fig. 2d (χ-scan) and Fig. 2e (2θ-scan). This shows significant changes in the line shape from 115 °C (N_{cybA}) to 105 °C (*phase-2*), which implies that the correlation length increases (or the SmA clusters grow) on going down from the nematic to *phase-2*. Hence, *phase-2* is identified as SmA phase.

At 102.5 °C, the texture starts to develop into a striped pattern (Fig. 1c). On further cooling down the sample to 100 °C, the texture suddenly changes to a nematic-like texture, which has lower viscosity than the SmA phase at higher temperatures and possesses thermal fluctuations. For the time being, this phase will be called *phase-3* (Fig. 1d). The texture looks very non-homogeneous (non-uniform) under the microscope. In a homeotropically aligned sample the transition from SmA to *phase-3* is indicated by the occurrence of birefringence (Fig. 1f), indicating the onset of phase biaxiality. Also this transition is not associated with a measurable enthalpy change. In the XRD pattern of the magnetically aligned sample the position of the small angle scattering remains centred on the meridian, which suggests that biaxiality in *phase-3* is not due to an onset of tilt (Fig. 2d and h). The intensity of the small angle scattering is slightly reduced and its *d*-value slightly increases compared to the SmA phase as shown in Fig. 2e. Layer thickness values, *d*, for different temperatures are 4.24 nm at 105 °C (SmA) and 4.31 nm at 98 °C (*phase-3*). This increase in the layer spacing is in line with the absence of tilt and was previously observed at the SmA to $SmAP_A$ transitions[27] as a more dense packing of the molecules in the polar phase requires alkyl chain stretching. Though the intensity of the small angle scattering is slightly reduced compared to that in the SmA phase, the line-shape for *phase-3* is distinctly different from the higher temperature N_{cybA} phase and

more similar to the SmA phase (see Fig. 2e), indicating a mesophase composed of relatively large clusters (CybA).

The optical behaviour of *phase-3* was checked for different planar alignment layers and in cells of thicknesses varying from 3 μm to 60 μm. But the phase existed irrespective of the alignment layer and of the cell thickness. On further cooling the sample to 97 °C, the material goes to *phase-4* whose POM texture is given in Fig. 1e. This phase shows sharp peaks at wide angle and at small angles; hence *phase-4* is identified as a crystalline mesophase (M).

To further understand the structure of *phase-3*, an electric field was applied perpendicular to the major director, to the cell containing the compound in planar alignment. The effect of electric field on the material in *phase-3* at 98 °C is shown in Fig. 3a–c. Under the electric field, the nematic-like less viscous non-homogeneous texture (Fig. 3a) goes to smectic-like textures (Fig. 3b and c). This texture remains the same for (+) and (−) dc fields. The polarisation reversal current was measured in *phase-3* in a 10 μm planar cell at a frequency of 40 Hz. The plot of current response to the applied triangular voltage is given in Fig. 3d. The phase shows a double switching current peak in half cycle of the applied voltage, indicating that the ground state structure of the mesophase is antiferroelectric.

The complex relative dielectric permittivity $\varepsilon^* = (\varepsilon' - j\varepsilon'')$; $j = \sqrt{-1}$ was measured on a planar aligned sample of 10 μm thickness. Fig. 4a shows the plot of ε' as a function of temperature for different frequencies, Fig. 4b shows the plot of dielectric loss, ε'', as a function of frequency between 200 Hz and 10 MHz for different temperatures and Fig. 4c gives the dependence of dielectric strength, $\delta\varepsilon$, and the relaxation frequency, f, of the observed processes on temperature. The $\delta\varepsilon$ and f are obtained by fitting the dielectric spectra to the Havriliak–Negami (H–N) equation. The H–N equation for j varying from 1 to n (number of relaxation processes) is given by eqn (1),

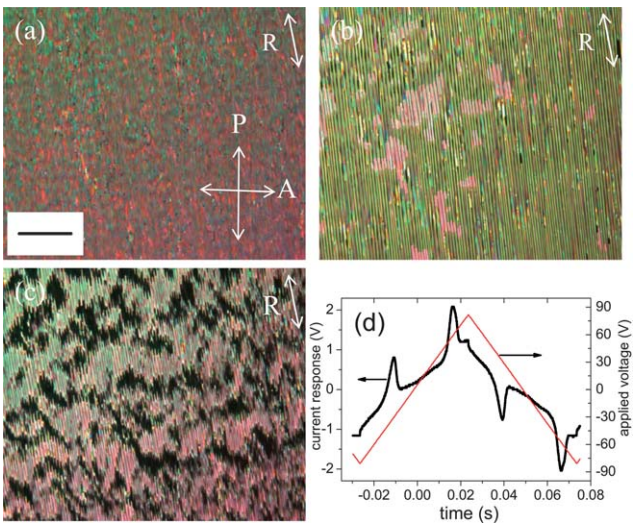

Fig. 3 *Phase-3* ($CybAP_A$) in a planar cell under the electric field, (a) 0 V, (b) 1.5 V μm^{-1}, (c) 3 V μm^{-1}. Frequency = 110 Hz, cell thickness = 10 μm and temperature = 98 °C. The length of the black line is 300 μm. P, A and R are the directions of polariser, analyser and rubbing. (d) Current response in a planar cell in *phase-3* ($CybAP_A$), $\boldsymbol{P}$ = 800 nC cm^{-2}. Frequency = 40 Hz, cell thickness = 10 μm.

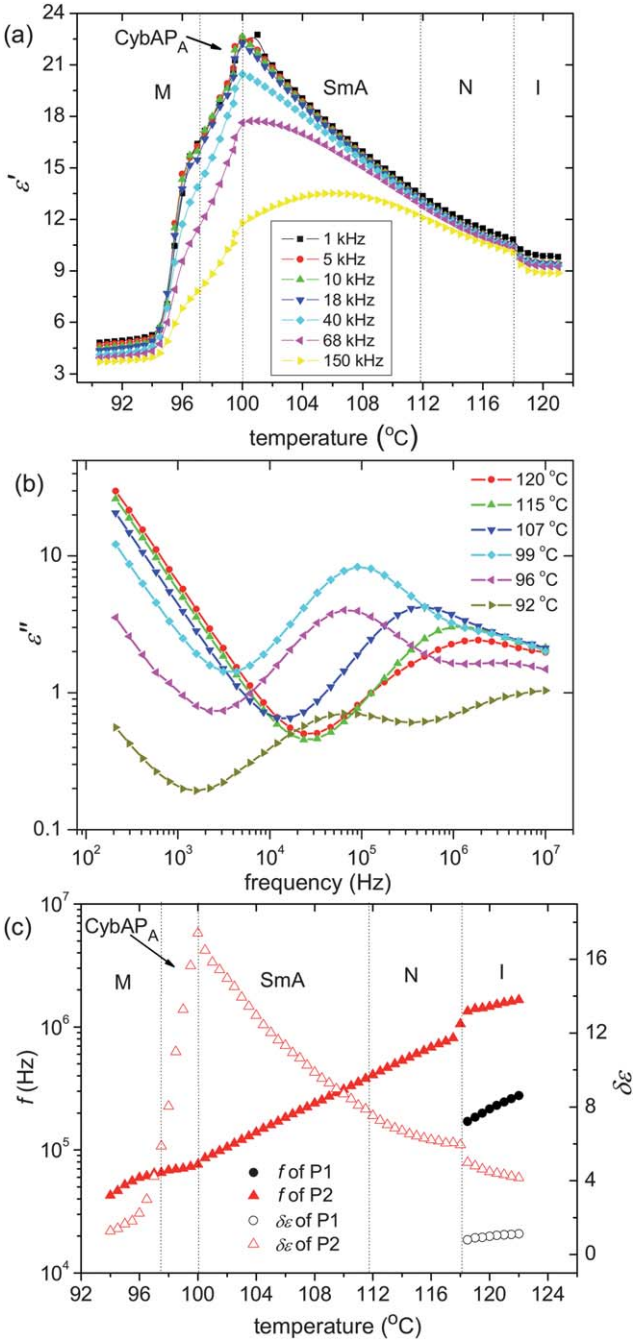

Fig. 4 Plot of (a) temperature dependence of ε' at different frequencies, (b) frequency dependence of ε'' at different temperatures, (c) relaxation frequency, f (closed symbols) and dielectric strength, $\delta\varepsilon$ (open symbols) *versus* temperature; cell thickness is 10 μm, alignment is planar.

where $\omega = 2f$ (f being the frequency in Hz) and ε_0 is the permittivity of free space.

$$\varepsilon^*(\omega) = \varepsilon' - i\varepsilon'' = \varepsilon_\infty + \sum_{j=1}^{n} \frac{\delta\varepsilon_i}{\left[1 + (i\omega\tau_j)^{\alpha_i}\right]^{\beta_i}} - \frac{i\sigma_{dc}}{\varepsilon_0\omega} \qquad (1)$$

where τ_j denotes the H–N relaxation time of the j^{th} relaxation process, $\delta\varepsilon_j$ is the dielectric relaxation strength, and α_j and β_j are the symmetric and asymmetric shape parameters of the j^{th} process, respectively. ε_∞ is the high frequency permittivity. The

term $\sigma_{dc}/\varepsilon_0\omega$ is the contribution of dc conductivity to ε''. The relaxation frequency of the j^{th} process, f_j, is related to the relaxation time τ_j by eqn (2). If β_j is unity, then according to eqn (2), $f_j = 1/2\tau_j$.

$$f_j = \frac{1}{2\pi\tau_j} + \left[\frac{\sin(\alpha_j\pi)}{2+2\beta_j}\right]^{1/\alpha_j}\left[\frac{\sin(\alpha_j\beta_j\pi)}{2+2\beta_j}\right]^{-1/\alpha_j} \quad (2)$$

From Fig. 4a we note that ε' increases significantly from the I → N_{cybA} → SmA → *phase-3* and reaches a maximum value at the phase transition temperature of SmA → *phase-3* (*i.e.*, at 1 kHz frequency, ε' changes from 9.5 in the isotropic phase to 23 at the SmA → *phase-3* transition temperature). A large increase in ε' indicates the appearance of strong dipolar correlations in *phase-3*. In the isotropic phase, two relaxation processes are observed in the measured frequency range. One is at the relaxation frequency, f = 300 kHz (say P1) and the second process at f = 1.25 MHz (say P2). After transition to the N_{cybA} phase, the lower frequency process, P1 disappears leaving only one process, P2, in the nematic phase. There is no appreciable difference observed in $\delta\varepsilon$ and f values of P2 at the N_{cybA} → SmA phase transition. $\delta\varepsilon$ increases rapidly as SmA → *phase-3* transition gets closer; *i.e.*, $\delta\varepsilon = 4$ in the isotropic phase, $\delta\varepsilon = 7$ at the isotropic to nematic phase transition temperature and $\delta\varepsilon = 17$ at the SmA → *phase-3* transition temperature. Also the f of P2 shows a discontinuity at the SmA → *phase-3* transition. The P2 could be attributed to the rotation around the long molecular axis and close to the SmA → *phase-3* phase transition, the rotation gains collective character.[8,28] For temperatures lower than for *phase-3*, another relaxation process (say P3) shows up. This mode could be due to some non-collective motion of molecules. The frequency of this process is close to the edge of the frequency window of the experiment; hence its origin cannot be ascertained.

From these results, we can conclude that *phase-3* is a CybA type phase, it is polar and antiferroelectrically switchable; hence it is designated as $CybAP_A$.

Fig. 5 shows a schematic representation of the molecular arrangement in the various mesophases. As mentioned before, *phase-1* is a uniaxial nematic phase with SmA cybotactic clusters (N_{cybA}) (Fig. 5a). As we go down in temperature, these clusters grow in size and fuse to layers in the SmA phase, (Fig. 5b). Then upon approaching $CybAP_A$, it seems that the layers become distorted again, which is shown in a slight decrease in the height of the layer reflection in Fig. 2d and e. This implies that there are relatively large clusters probably elongated clusters present in this phase (Fig. 5c). There is a slight shift of the d values to larger

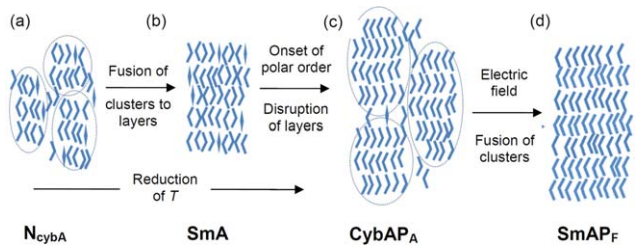

Fig. 5 Schematic representation of molecular arrangements in (a) N_{cybA}, (b) SmA and (c) in $CybP_A$ phases; (d) $SmAP_F$ state induced by applying an electric field to the $CybAP_A$ phase.

values from 105 °C (SmA) to 98 °C ($CybAP_A$). This could be due to a denser packing of the aromatics in the $CybAP_A$ phase. The denser packing of the aromatics is associated with the onset of phase biaxiality and polar order. Simultaneously, there seems to be an increased layer frustration due to a growing mismatch of the interfacial area required by the densely packed aromatics and the fluid alkyl chains. Hence, the layers break again at the transition from SmA to $CybAP_A$, which leads to an increased fluidity and a nematic-like appearance of the $CybAP_A$ phase. On lowering the temperature further the sample starts crystallising or forms a crystalline mesophase, M.

3. Experimental methods

The cells were made of chemically etched, indium tin oxide (ITO) coated glass plates with a sheet resistance of 20 Ω/□. The conducting inner surfaces were spin coated with a polyimide RN1175 (Nissan Chemicals, Japan) and rubbed parallel for planar alignment. For homeotropic alignment, the substrates were coated with a polymer AL60702 (JSR Korea). The cell thickness was controlled by polymer spacers. The sample was filled in the isotropic phase and cooled down slowly. The sample temperature was maintained by placing the cell on a hot stage whose temperature was controlled by a Eurotherm-2604 temperature controller with an accuracy of ±0.01 °C. A polarising optical microscope (Olympus-BX51) and a signal generator connected to an amplifier have been used for recording the texture and to study the electro-optical behaviour. The polarising switching current was measured across a resistor of 5 kΩ using the standard triangular wave technique.

X-Ray diffraction studies have been carried out using a 2D detector (HI-Star, Siemens AG). Uniform alignment of the sample was achieved by inserting the capillary containing the material in the magnetic field ($\boldsymbol{B}$ = 1 T). The liquid crystal alignment is maintained by the slow cooling of the sample in a magnetic field. The exposure time for each temperature was 30 min. Dielectric measurements were carried out using a Novocontrol Alpha High Resolution Dielectric Analyser (Novocontrol GmbH, Germany). The real and imaginary parts of the complex relative permittivity were measured in the frequency range of 200 Hz to 10 MHz on slow cooling of the sample.

4. Conclusions

We have characterised a new phase of a bent-core liquid crystal by means of polarising optical microscopy, electro-optics, X-ray and dielectric spectroscopy. It occurs below a SmA phase and appears like a nematic phase under the polarising microscope but transforms to a smectic texture under an applied electric field and shows tristable antiferroelectric switching. The phase structure has been confirmed by X-ray diffraction to consist of smectic clusters with a non-tilted organisation of the molecules in the clusters. The dielectric study also indicates strong dipolar correlation in this phase. The phase is the non-tilted and polar version of the previously reported CybC phase[19] and is labelled as $CybAP_A$. Since the $CybAP_A$ phase is cybotactic in character, the smectic and ferroelectric version of this phase is obtained on applying an electric field. This represents a significant step forward to biaxiality in nematic phases of bent-core molecules. If

further molecular design would allow reducing the size of the $SmAP_A$ clusters to that found in N_{CybA} phases without loss of polar order one would get a polar biaxial nematic phase of the orthorhombic type (N_{cybAPA}). Such a cybotactic nematic phase would be of significant interest for fast switching display applications.

Acknowledgements

This work was supported by the EU within the FP7 funded collaborative project BIND (grant no. 216025).

Notes and references

1 R. A. Reddy and C. Tschierske, *J. Mater. Chem.*, 2006, **16**, 907; H. Takezoe and Y. Takanishi, *Jpn. J. Appl. Phys.*, 2006, **45**, 597.
2 T. Sekine, T. Niori, J. Watanabe, T. Furukawa, S. W. Choi and H. Takezoe, *J. Mater. Chem.*, 1997, **7**, 1307.
3 T. Niori, T. Sekine, J. Watanabe, T. Furukawa and H. Takezoe, *J. Mater. Chem.*, 1996, **6**, 1231.
4 H. R. Brand, P. E. Cladis and H. Pleiner, *Macromolecules*, 1992, **25**, 7223.
5 D. Pociecha, M. Čepič, E. Górecka and J. Mieczkowski, *Phys. Rev. Lett.*, 2003, **91**, 185501.
6 A. Eremin, S. Diele, G. Pelzl, H. Nádasi, W. Weissflog, J. Salfetnikova and H. Kresse, *Phys. Rev. E: Stat., Nonlinear, Soft Matter Phys.*, 2001, **64**, 051707.
7 U. Dunemann, M. W. Schröder, R. A. Reddy and C. Tschierske, *J. Mater. Chem.*, 2005, **15**, 4051.
8 D. Pociecha, M. Čepič, E. Górecka, N. Vaupotič, K. Gomola and J. Mieczkowski, *Phys. Rev. E: Stat., Nonlinear, Soft Matter Phys.*, 2005, **72**, 060701.
9 H. N. S. Murthy and B. K. Sadashiva, *Liq. Cryst.*, 2004, **31**, 567.
10 L. Guo, S. Dhara, B. K. Sadashiva, S. Radhika, R. Pratibha, Y. Shimbo, F. Araoka, K. Ishikawa and H. Takezoe, *Phys. Rev. E: Stat., Nonlinear, Soft Matter Phys.*, 2010, **81**, 011703.
11 R. A. Reddy, C. Zhu, R. Shao, E. Korblova, T. Gong, Y. Shen, E. Garcia, M. A. Glaser, J. E. Maclennan, D. M. Walba and N. A. Clark, *Science*, 2011, **332**, 72.
12 B. K. Sadashiva, R. Amaranatha Reddy, R. Pratibha and N. V. Madhusudana, *J. Mater. Chem.*, 2002, **12**, 943.
13 C. V. Yelamaggad, I. S. Shashikala, D. S. S. Rao, G. G. Nair and S. K. Prasad, *J. Mater. Chem.*, 2006, **16**, 4099.
14 C. V. Yelamaggad, I. S. Shashikala, V. P. Tamilenthi, D. S. S. Rao, G. G. Nair and S. K. Prasad, *J. Mater. Chem.*, 2008, **18**, 2096.
15 M. J. Freiser, *Phys. Rev. Lett.*, 1970, **24**, 1041.
16 A. G. Vanakaras and D. J. Photinos, *J. Chem. Phys.*, 2008, **128**, 154512.
17 C. Tschierske and D. J. Photinos, *J. Mater. Chem.*, 2010, **20**, 4263.
18 O. Franscescangeli and E. T. Samulski, *Soft Matter*, 2010, **6**, 2413.
19 C. Keith, A. Lehmann, U. Baumeister, M. Prehm and C. Tschierske, *Soft Matter*, 2010, **6**, 1704.
20 M. W. Schröder, S. Diele, G. Pelzl, U. Dunemann, H. Kresse and W. Weissflog, *J. Mater. Chem.*, 2003, **13**, 1877.
21 J. L. Serrano, T. Sierra, Y. Gonzalez, C. Bolm, K. Weickhardt, A. Magnus and G. Moll, *J. Am. Chem. Soc.*, 1995, **117**, 8312.
22 R. Achten, E. A. W. Smits, R. A. Reddy, M. Giesbers, A. T. M. Marcelis and E. J. R. Sudhölter, *Liq. Cryst.*, 2006, **33**, 57.
23 R. A. Reddy, V. A. Raghunathan and B. K. Sadashiva, *Chem. Mater.*, 2005, **17**, 274.
24 R. A. Reddy and B. K. Sadashiva, *J. Mater. Chem.*, 2002, **12**, 2627.
25 R. A. Reddy and B. K. Sadashiva, *Liq. Cryst.*, 2003, **30**, 1031.
26 L. Kovalenko, M. W. Schröder, R. A. Reddy, S. Diele, G. Pelzl and W. Weissflog, *Liq. Cryst.*, 2005, **32**, 857.
27 C. Keith, M. Prehm, Y. P. Panarin, J. K. Vij and C. Tschierske, *Chem. Commun.*, 2010, **46**, 3702.
28 H. Kresse, H. Schlacken, U. Dunemann, M. W. Schröder, G. Pelzl and W. Weissflog, *Liq. Cryst.*, 2002, **29**, 1509.